Tailoring the Dispersion of Plasmonic Nanorods To Realize Broadband Optical Meta-Waveplates

ARTICLE *in* NANO LETTERS · FEBRUARY 2013

Impact Factor: 13.59 · DOI: 10.1021/nl304392b · Source: PubMed

NANO LETTERS

Letter

pubs.acs.org/NanoLett

Tailoring the Dispersion of Plasmonic Nanorods To Realize Broadband Optical Meta-Waveplates

Yang Zhao and Andrea Alù*

Department of Electrical and Computer Engineering, The University of Texas at Austin, Austin, Texas 78712, United States

ABSTRACT: The response of optical metasurfaces is usually narrowband, and mechanisms to increase their bandwidth often clash with causality and passivity constraints of materials. Here we are able to theoretically and experimentally demonstrate that broadband, strong polarization conversion and quarter-wave plate functionality may be achieved using a single, ultrathin planar metasurface in the visible regime. Our realized sample is based on interleaved silver nanorods with properly tailored frequency dispersion that introduce an abrupt flat 90° phase shift for orthogonal polarizations over a thickness of few tens of nanometers, achieving achromatic quarter-wave plate behavior covering a good portion of the visible spectrum. Analogous design principles are extended to cover the entire visible spectrum and beyond.

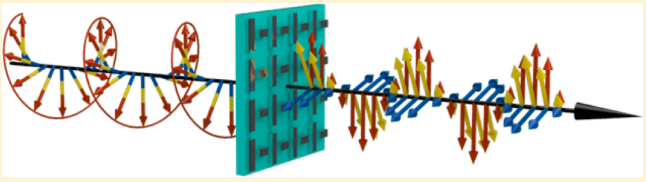

KEYWORDS: *Plasmonics, metasurface, polarization, color filter, nanophotonics, waveplate*

In nature, a few biological species rely on circularly polarized vision[1] for sensing, signaling, orientation, and navigation. In contrast, human eyes can only distinguish color and intensity of light, whereas polarization is not detected. Nevertheless, there has been a long interest in polarization assisted vision. As early as in 1967, Lythgoe and Hemmings proposed that polarization could be used to assist in visualizing transparent or obscure targets in water.[2] Recent studies have shown that polarization imaging may help revealing tumor boundaries which were undetectable under conventional medical imaging modalities.[3] Compared to linear polarization, circular polarization is particularly important to sense DNA and certain proteins with chiral geometry,[4] and it is inherently more robust to arbitrary reflection and scattering in complex environments. These applications ultimately require the generation of controllable polarized light and ready integration into existing compact imaging and microfluidic systems.

Conventional circular polarization is obtained by stacking a linear polarizer with bulky quarter-wave plates made by birefringent materials. This configuration cannot be easily integrated in a nanophotonic system, and it is inherently narrow bandwidth, as conventional quarter-wave plates rely on wavelength-dependent dispersion of the birefringence phenomenon. For this reason, metamaterials have been recently explored and proposed to realize quarter-wave plates and circular polarizers in compact, planarized, and easily integrated designs.[5−11] Especially interesting in this context are plasmonic metasurfaces,[12−18] which are able to induce strong electron−photon interaction within a thickness of few nanometers, as proposed by several groups both theoretically and experimentally.[5−11,19−21] As in the case of metamaterials, their extreme thickness and subwavelength resonant effects limit their functionality to a narrow bandwidth, with evident constraints on their impact and applicability in realistic optical systems. Broadband circular polarization conversion has been recently realized in 3D optical metamaterials[12,22] using helical or twisted arrangements of resonant inclusions. In a very recent study,[23] broadband polarization conversion was realized over a much reduced thickness in the mid-IR region. This effect relies on the cross-polarization properties of optical phased antenna arrays, which inherently limits the overall conversion efficiency. In addition, the output circularly polarized wave is radiated at an oblique angle, whose radiation direction may vary for different frequencies, posing limitations to its practical applicability. In the following, we show that broadband quarter-wave plate operation at normal incidence with large conversion efficiency based on the dominant diffraction order can be achieved using a single, ultrathin patterned plasmonic surface, only few nanometers thick, by properly tailoring the frequency dispersion of closely spaced silver nanorods operated off resonance.

Waveplate functionality may be obtained over a thin surface by introducing an abrupt jump in the phase of transmitted light, tailored to be a function of the impinging polarization. This may be achieved in the form of a localized birefringence using anisotropic nanoparticle arrays.[5,10,21,24] A nanorod is the simplest form of anisotropic nanoparticle, as it mainly interacts with the impinging polarization parallel to its axis. When plasmonic effects are considered, resonant dipolar response may be obtained for a length significantly shorter than the excitation wavelength, which may be further controlled by the rod thickness that modulates its surface plasmon properties. The corresponding phase of the induced dipole moment shows fast variations around this resonance wavelength, essentially flipping by up to 180°.

Received: November 28, 2012
Revised: February 3, 2013
Published: February 5, 2013

   dx.doi.org/10.1021/nl304392b | *Nano Lett.* 2013, 13, 1086−1091

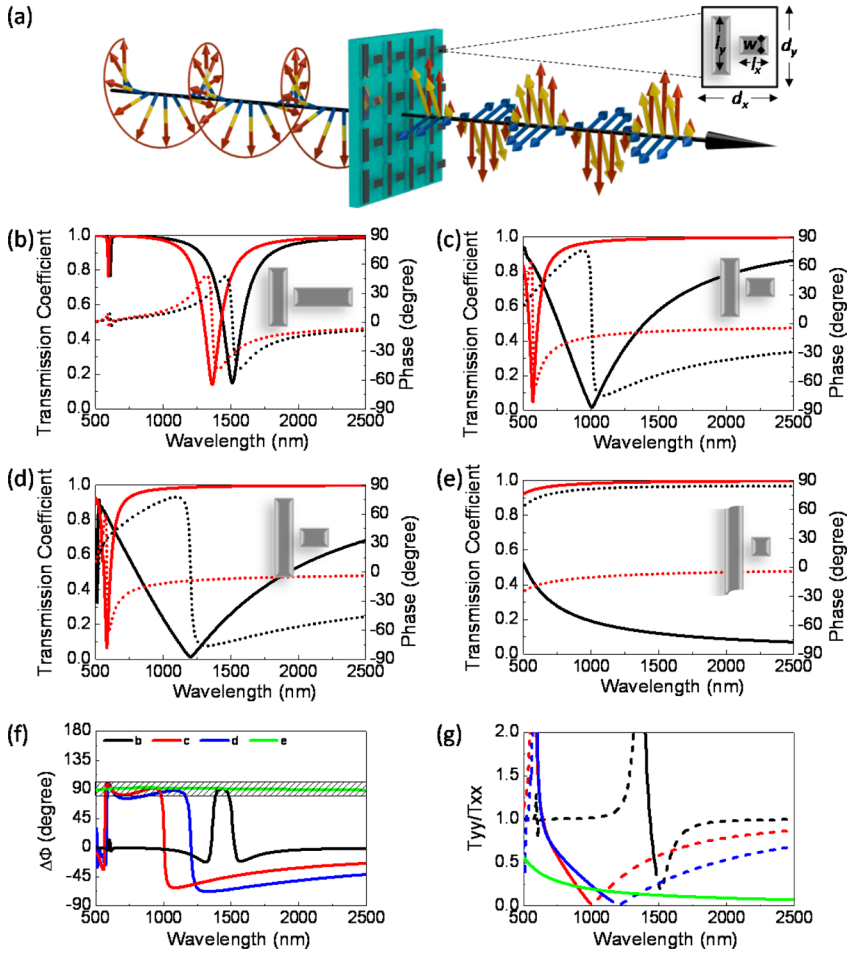

Figure 1. (a) Schematic illustration of the functionality of the proposed nanodevice with broadband circular excitation: the transmitted beam is linearly polarized at different angles as a function of the impinging wavelength, covering a broad spectrum. The inset shows the configuration of the unit cell. (b) Transmission coefficients for orthogonal linear polarizations: magnitude (solid curves), phase (dotted). Geometry of the metasurface: l_x = 160 nm, l_y = 160 nm, thickness z = 8 nm, w = 20 nm, all gaps between dipoles are kept at 10 nm. (c) Transmission coefficients for the second design, similar to b, except that l_x = 60 nm, l_y = 160 nm ,and z = 45 nm. (d) Similar to the previous panels, but with l_x = 60 nm, l_y = 240 nm, and z = 50 nm. (e) Extreme design for ultrabroad bandwidth: the vertical rods are connected into a continuous wire with width w = 20 nm, the horizontal rod is a square with side dimensions l_x = 10 nm and z = 60 nm. (f) Extracted phase difference between the two orthogonal linear excitations for the three designs. The shadowed area marks the acceptable phase difference that can realize a quarter-wave plate. (g) Amplitude ratio of the transmitted fields polarized along the vertical and horizontal directions. Black, red, blue, and green curves correspond to the designs in panels b, c, d, and e, respectively. The solid portion of each curve corresponds to the range over which the phase difference ΔΦ is near 90°.

Consider now two orthogonally patterned nanorods with lengths l_x and l_y arranged in a planar rectangular array with periods d_x and d_y, as we have theoretically considered[25] and shown in the inset of Figure 1a. Each nanorod interacts with the polarization parallel to the rod axis, with a wavelength response determined by the resonant dispersion of the rods and by the array interaction. Transmission may be easily related to the polarizability tensor $\boldsymbol{\alpha}$ of the rods and the interaction dyadic $\mathbf{C}_{\text{int}}$ of the array.[26−28] The rod polarizability may be well-approximated by the three-axial ellipsoid quasi-static polarizability with semiaxes $w/2$, $z/2$, and $l/2$, which provides a diagonal tensor $\boldsymbol{\alpha}$ with elements $\alpha_{ii} = \pi/8\ wzl\ (\varepsilon_{\text{Ag}} - \varepsilon_{\text{m}})/[3\varepsilon_{\text{m}} + 3L_i(\varepsilon_{\text{Ag}} - \varepsilon_{\text{m}})]$, i = **x**, **y**, and **z**, where L_i is the shape factor, along with the width w, the thickness z, and the length l of the nanorod, and ε_{Ag} and ε_{m} are the permittivities of the rod and of the surrounding medium, respectively.[29] As long as the array periods are smaller than the wavelength, we can model the surface with its averaged transverse polarization current, and the corresponding transmission matrix can be calculated through the formula:

$$\mathbf{T} = \begin{pmatrix} T_{xx} & 0 \\ 0 & T_{yy} \end{pmatrix} = \begin{pmatrix} 1 - \dfrac{j\mu_0 \pi f c}{d_x d_y} \dfrac{\alpha_{xx}}{1 - C_{xx}\alpha_{xx}} & 0 \\ 0 & 1 - \dfrac{j\mu_0 \pi f c}{d_x d_y} \dfrac{\alpha_{yy}}{1 - C_{yy}\alpha_{yy}} \end{pmatrix}$$

where f is the frequency of operation, c is the speed of light in vacuum, and μ_0 is the permeability of free space. The above formula allows tailoring amplitude and phase of the transmission coefficients in the two orthogonal polarizations as a function of the rod geometry and array periods.[29] Our goal is to tailor the polarizability dispersion of the nanorods to realize a flat phase difference between T_{xx} and T_{yy} over frequency.

Consider a first scenario in which the two nanorods within the unit cell have the same length $l_x = l_y$ = 160 nm, width w = 20 nm, and thickness z = 8 nm, with array periods d_x = 200 nm

dx.doi.org/10.1021/nl304392b | Nano Lett. 2013, 13, 1086−1091

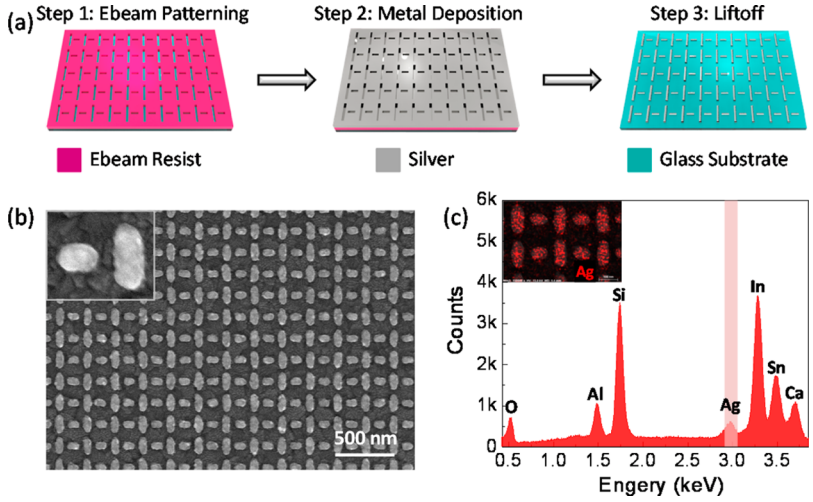

Figure 2. (a) Nanofabrication flow. (b) Scanning electron microscope (SEM) images of silver nanodipoles on ITO coated glass. The inset shows the dimension of the two orthogonal nanorods: l_x = 95 nm, w_x = 65 nm, l_y = 150 nm, w_y = 60 nm. (c) Energy dispersive X-ray spectrum (EDS) of the structure showing the constituent materials, where Al and Ca are dopants of the glass substrate. The inset shows the mapping of silver (red) superimposed to the SEM image.

and d_y = 170 nm (inset of Figure 1b). The corresponding transmission coefficients for impinging orthogonal linear polarizations along the rods are shown in Figure 1b, with two pronounced resonant dips, obtained using full wave numerical simulations. Despite the rods having the same dimensions, the different array interaction in the two polarizations produces a slight detuning of the two resonances.[30,31] For this specific design, at the intersection of the two transmission curves between resonant dips we meet the conditions to realize an ultrathin quarter-wave plate,[25] i.e., a phase difference $\Delta\Phi = \Phi_{xx} - \Phi_{yy}$ for the transmission coefficients equal to 90°, which is plotted over wavelength in Figure 1f (black line). This was obtained by properly tuning the rod thickness z to modify the surface plasmon propagation along the rods and induce the required phase shift. Although this design provides a quarter-wave plate functionality, it only covers a very narrow range of wavelengths between the array resonances.

To broaden this effect, we consider detuning one of the two resonances in Figure 1c, by shortening one rod to l_x = 60 nm, which shifts its resonance to the visible range. By properly adjusting the thickness to z = 45 nm, we are able to ensure that the phase dispersion curves (dashed lines in Figure 1c) follow each other closely in the range between the two resonances, an effect that is reflected into a flat phase difference $\Delta\Phi$ (Figure 1f, red line) around 90° over a broad range of wavelengths in the visible regime.

Further increasing the distance between the two resonances, by pushing l_y to 240 nm and tuning z = 50 nm (Figure 1d), provides an even broader bandwidth over which the phase is around 90°. In this case the two phase dispersion curves start slightly diverging from each other near the shorter rod resonance, which moderately affects the performance at shorter wavelengths. In spite of that, the waveplate still covers a fairly flat cumulative bandwidth of ~570 nm.

To push this concept even further, we consider the final design in Figure 1e, in which the vertical rods are joined, and the horizontal rods are reduced to a square with l_x = 10 nm. This solution is necessary to eliminate part of the unwanted phase dispersion by effectively moving the vertical resonance to very long wavelengths. In this case, the presence of the small square nanoantenna is still necessary, since it allows interacting with the horizontal polarization and control the phase difference. Without it the elongated wires would essentially form a linear polarizer, offering much less polarization control.[32] By controlling the coupling between the long wire and the small dipole, the phase difference $\Delta\Phi$ may be made extremely flat at 90° for the specific thickness z = 60 nm over a huge spectrum (Figure 1f, green line), spanning the entire visible and near-IR regions.

It is interesting to observe how, by simply tuning the location of the two orthogonal array resonances and choosing a suitable subwavelength thickness to modify the phase dispersion of the induced surface plasmons supported by the rods, we are able to essentially create achromatic waveplate functionality over an ultrabroad wavelength range. Contrary to a conventional birefringent slab, the optimal thickness increases with larger anisotropy of the surface, a counterintuitive effect that is associated with the fact that a plasmonic nanorod resonance moves to shorter wavelengths when its thickness is reduced.[33]

We notice that, within the bandwidth of operation, the ratio of transmitted amplitudes for the two orthogonal linear polarizations varies in all of the proposed designs, as shown in Figure 1g, due to the different amplitude dispersion of the two rods, one operated past its resonance, one before it. In this panel, the solid portion of each curve corresponds to the wavelength range of interest, over which the phase difference $\Delta\Phi$ is near 90°. This amplitude variation reflects into a frequency dispersion of the effective fast and slow axes of the proposed waveplate.[25] For circular polarization excitation, the transmitted beam is always linearly polarized, but at an angle that depends on the wavelength of excitation (color), as schematically illustrated in Figure 1a and experimentally demonstrated in the following.

To test and experimentally verify the possibilities offered by this phenomenon, we have experimentally realized the design of Figure 1c by patterning orthogonal arrays of silver nanorods on a silica substrate. Due to the resolution limitation of our electron-beam lithography tools, we have slightly released the minimum dimensions of our initial design. In addition, we have taken into account the effect of the substrate, which red-shifts the resonances and reduces the phase difference $\Delta\Phi$. To

dx.doi.org/10.1021/nl304392b | Nano Lett. 2013, 13, 1086–1091

counterbalance this effect, we slightly adjusted the aspect ratio of each nanorod to optimize the bandwidth of operation.

The fabrication flow is shown in Figure 2a. A one inch by one inch sized optical flat glass with 0.7 mm thickness (C1737-0107, Corning low-alkaline earth from Delta Technologies) precoated with indium−tin oxide (ITO) was used as the substrate. Positive tone ebeam resist ZEP 520 (ZEON, Japan) was first diluted with anisole (99%, Sigma-Aldrich), then spun onto the substrate to obtain a thickness of 100 nm with less than 5 nm thickness variation, characterized using spectroscopic ellipsometry (J.A. Woollam M-2000 DI ellipsometer). The pattern was written using a JBX-6000FS/E ebeam aligner at an accelerating voltage of 50 kV. After exposure, the sample was developed in emyl acetate (ZEON, Japan). A 2 nm germanium adhesive layer and 55 nm silver layer were sequentially deposited onto the sample using a CHA ebeam evaporator. The deposition rate of the germanium layer was precisely controlled under 0.2 Å/s to minimize the thickness inhomogeneity during metallization.[34] Then, the sample underwent a liftoff process in *N*-methyl-2-pyrrolidone (Sigma-Aldrich) to complete the device fabrication.

Figure 2b shows the scanning electron microscope (SEM) image of the fabricated metasurface, which is composed of interleaved nanorods with a lateral length l_x = 95 nm, a vertical length l_y = 150 nm, a horizontal width w_x = 65 nm, and a vertical width w_y = 60 nm. The nanorods are embedded within a 240 nm × 190 nm rectangular lattice with interparticle spacing of 40 nm. An energy dispersive X-ray spectrum (EDS) is shown in Figure 2c to reveal the constituent materials of the sample. The impurity lines in the EDS come from the ITO coated glass substrate.

We first excited the metasurface with monochromatic circularly polarized light generated using a white light source sequentially passing through a spectrometer and polarizing optics. A Halogen broadband light source was coupled through an optical fiber into the spectrometer (Princeton instrument SpectraPro-2500i), which is controlled using a Labview system to set the scan wavelength. The circular excitation was generated by passing the output light from the spectrometer sequentially through a linear polarizer (Thorlabs LPVIS050) and a broadband quarter-wave plate (Thorlabs AQWP05M-980). To obtain a moderate intensity at the output to meet the sensitivity of the detector at higher frequencies, instead of a collimated beam, a slightly converging beam with a solid angle of 10° was formed with a long focal length lens to focus the beam onto the sample. A second analyzer (Thorlabs LPVIS050) was used after the sample to check the angular response of the device. The final output was then fed into an InGaAs detector (Princeton instrument model ID441-C). Wavelengths were scanned from 620 to 900 nm with a 20 nm interval, and the output intensity was recorded at each wavelength as a function of the polarizing angle of a second linear polarizer situated in front of the detector and normalized as shown in Figure 3a. A strong dependence of the measured intensity as a function of the linear polarization angle is achieved, confirming a large degree of linear polarization and extinction ratio over the whole bandwidth of analysis. The dips of each curve, which would ideally approach zero in our simulations from 620 to 830 nm, show a residual nonzero value, possibly associated with the absorption of the germanium adhesive layer, degradation due to material oxidation, and/or small fabrication imperfections.

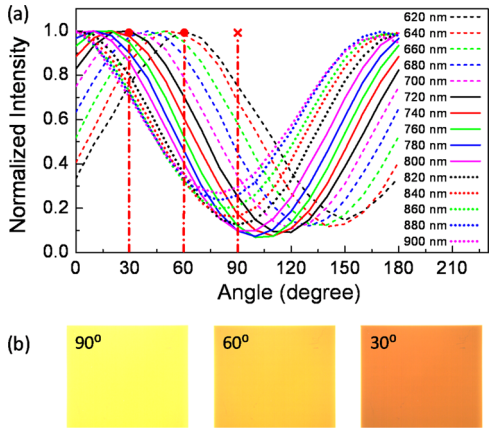

Figure 3. (a) Normalized amplitude measured at the output of the device for circularly polarized input by rotating a linear polarizer in front of the detector. (b) Polarizing microscope image of the device for white light illumination (field of view: 1 mm × 0.86 mm) showing color tuning for three different polarization angles in front of the detector.

In Figure 3a we also show three vertical dash−dot lines corresponding to three specific observation angles for our second linear polarizer at 90°, 60° and 30°. In Figure 3b we show the corresponding image obtained under a polarizing microscope with white light illumination. The color change by rotating the microscope polarizer reflects the wavelength of maximum transmission for the specific angle, as indicated by the dots in Figure 3a, providing an interesting functionality as color filter, as proposed in a recent paper for a related plasmonic metasurface geometry.[35] Due to the low sensitivity of our detector at 580 nm, the corresponding curve for the maximum at 90° polarization was not recorded in Figure 3a (marked as a "cross" at the end of the corresponding vertical line), but a clear yellow color is observed in the microscope image, ensuring that the polarization properties extend to the yellow range.

From the measurements of Figure 3a, we have extracted the overall degree of linear polarization and corresponding angle of linear polarization of our device for circular polarization excitation, shown in Figure 4a. There is a broad range of wavelengths over which the degree of linear polarization is remarkably large, in good agreement with full-wave simulations (Figure 4b). Our simulations were performed by assuming nondispersive ITO (ε_{ITO} = 2.56) and silica (ε_{SiO_2} = 2.1) and a Drude model[36] for silver with $\varepsilon_{Ag} = \varepsilon_0 [\varepsilon_\infty - (f_p^2)/(f(f - i\gamma))]$, ε_∞ = 5, f_p = 2.175 PHz, and γ = 4.35 THz. As highlighted above, the angle of linear polarization changes with wavelength, and at $\lambda \cong$ 670 nm it is 45°, which implies that the effective optical axes of the waveplate align with the orthogonal nanorods, achieving the functionality originally described in ref 25. At this specific wavelength, the two transmission curves for linear polarization excitation intersect, as we experimentally confirmed in Figure 4c using linearly polarized excitation. The measurement was obtained by scanning the wavelength from 575 to 925 nm at a 2 nm resolution. Despite the detector's lower sensitivity at wavelengths shorter than 620 nm, the measured curves still agree well with our simulations (Figure 4d) and indicate that, despite some inevitable thickness inhomogeneity and material losses, which reduce the resonance strength at shorter wavelengths, the realized device provides broadband quarter-wave plate functionality over an ultrathin

dx.doi.org/10.1021/nl304392b | *Nano Lett.* 2013, 13, 1086−1091

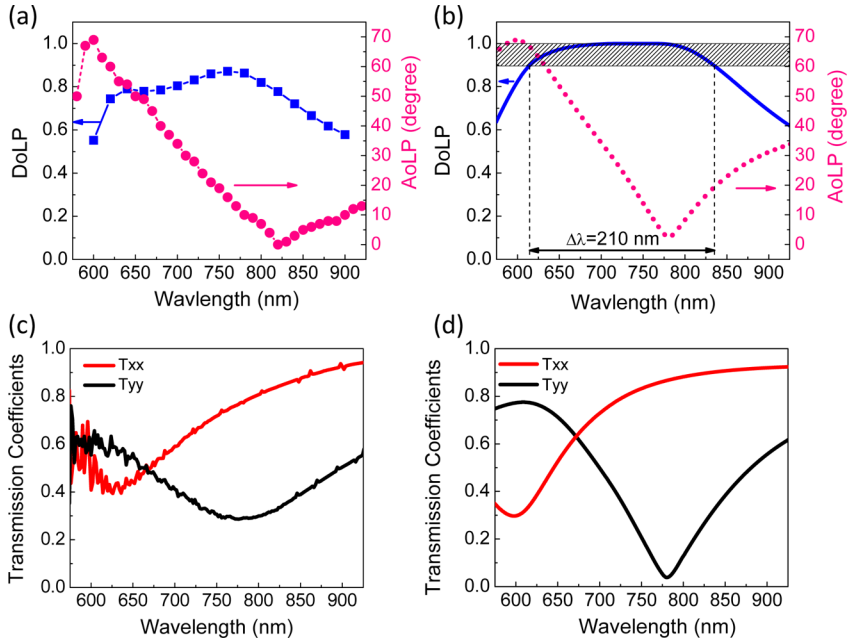

Figure 4. (a) Experimentally measured degree of linear polarization (DoLP) and angle linear polarization (AoLP) for circularly polarized excitation. (b) Corresponding full wave simulations for panel a. (c) Experimental measurement of the transmission coefficients for linearly polarized excitation along the two nanorod axes. (d) Corresponding full wave simulations for panel c.

thickness. Compared to other recently realized devices based on V-shaped nanoantennas,[20] this concept provides broader bandwidth of operation and larger coupling efficiency. Since our operation is based on the dominant diffraction order of the periodic array, we ensure a peak conversion efficiency approaching 50% over the entire wavelength of operation, which is only limited by material loss.

In summary, we have shown that broadband polarization conversion and quarter-wave plate functionality may be achieved over a single ultrathin plasmonic metasurface with few tens of nanometers thickness, by tailoring the frequency dispersion of silver nanorods operated off-resonance. The proposed metasurface concept can provide broadband full control of the transmitted phase at the nanoscale, and it may be extended to different values of phase retardation, even locally varied over the surface, and span a broad spectrum in the visible, near-infrared, and even THz range. These concepts may have a profound impact on novel integrated nanophotonic devices, as a new platform for biosensing, polarization imaging, enhanced night vision devices, modulators, phase retarders, nanoantennas, and nanotransmit-arrays.

AUTHOR INFORMATION

Corresponding Author

*Telephone: (512) 471-5922. Fax: (512) 471-6598. E-mail: alu@mail.utexas.edu.

Notes

The authors declare no competing financial interest.

ACKNOWLEDGMENTS

The authors would like to thank H. Giessen and M. Belkin for useful discussions and S. Bank for some of the characterization equipment. This work has been supported by the ONR MURI grant No. N00014-10-1-0942 and the Norman Hackerman Advanced Research Program.

REFERENCES

(1) Cronin, T. W.; Shashar, N.; Caldwell, R. L.; Marshall, J.; Cheroske, A. G.; Chiou, T. H. *Integr. Comput. Biol.* **2003**, *43*, 549−558.
(2) Lythgoe, J. N.; Hemmings, C. C. *Nature* **1967**, *213*, 893−894.
(3) Yaroslavsky, A. N.; Neel, V.; Anderson, R. R. *J. Invest. Dermatol.* **2003**, *121*, 259−266.
(4) Sparks, W. B.; Hough, J.; Germer, T. A.; Chen, F.; DasSarma, S.; DasSarma, P.; Robb, F. T.; Manset, N.; Kolokolova, L.; Reid, N.; Macchetto, F. D.; Martin, W. *Proc. Natl. Acad. Sci. U.S.A.* **2009**, *106*, 7816−7821.
(5) Baida, F. I.; Boutria, M.; Oussaid, R.; Van Labeke, D. *Phys. Rev. B* **2011**, *84*, 035107.
(6) Papakostas, A.; Potts, A.; Bagnall, D. M.; Prosvirnin, S. L.; Coles, H. J.; Zheludev, N. I. *Phys. Rev. Lett.* **2003**, *90*, 107404.
(7) Biagioni, P.; Huang, J. S.; Duo, L.; Finazzi, M.; Hecht, B. *Phys. Rev. Lett.* **2009**, *102*, 256801.
(8) Khoo, E. H.; Li, E. P.; Crozier, K. B. *Opt. Lett.* **2011**, *36*, 2498−2500.
(9) Pors, A.; Nielsen, M. G.; Della Valle, G.; Willatzen, M.; Albrektsen, O.; Bozhevolnyi, S. I. *Opt. Lett.* **2011**, *36*, 1626−1628.
(10) Ogut, E.; Sendur, K. *Appl. Phys. Lett.* **2010**, *96*, 141104.
(11) Drezet, A.; Genet, C.; Ebbesen, T. W. *Phys. Rev. Lett.* **2008**, *101*, 043902.
(12) Gansel, J. K.; Thiel, M.; Rill, M. S.; Decker, M.; Bade, K.; Saile, V.; Von Freymann, G.; Linden, S.; Wegener, M. *Science* **2009**, *325*, 1513−1515.
(13) Jen, Y.-J.; Lakhtakia, A.; Yu, C.-W.; Lin, C.-F.; Lin, M.-J.; Wang, S.-H.; Lai, J.-R. *Nat. Commun.* **2011**, *2*, 363.
(14) Shalaev, V. M. *Nat. Photonics* **2007**, *1*, 41−48.
(15) Fedotov, V. A.; Schwanecke, A. S.; Zheludev, N. I.; Khardikov, V. V.; Prosvirnin, S. L. *Nano Lett.* **2007**, *7*, 1996−1999.
(16) Decker, M.; Ruther, M.; Kriegler, C. E.; Zhou, J.; Soukoulis, C. M.; Linden, S.; Wegener, M. *Opt. Lett.* **2009**, *34*, 2501−2503.
(17) Zhou, J.; Dong, J.; Wang, B.; Koschny, T.; Kafesaki, M.; Soukoulis, C. M. *Phys. Rev. B* **2009**, *79*, 121104.
(18) Alù, A.; Yaghjian, A. D.; Shore, R. A.; Silveirinha, M. G. *Phys. Rev. B* **2011**, *84*, 054305.
(19) Hsu, S.-Y.; Lee, K.-L.; Lin, E.-H.; Lee, M.-C.; Wei, P.-K. *Appl. Phys. Lett.* **2009**, *95*, 013105.

(20) Kats, M. A.; Genevet, P.; Aoust, G.; Yu, N.; Blanchard, R.; Aieta, F.; Gaburro, Z.; Capasso, F. *Proc. Natl. Acad. Sci. U.S.A.* **2012**, *109*, 12364−12368.
(21) Li, T.; Liu, H.; Wang, S.-M.; Yin, X.-G.; Wang, F.-M.; Zhu, S.-N.; Zhang, X. *Appl. Phys. Lett.* **2008**, *93*, 021110.
(22) Zhao, Y.; Belkin, M. A.; Alù, A. *Nat. Commun.* **2012**, *3*, 870.
(23) Yu, N.; Aieta, F.; Genevet, P.; Kats, M. A.; Gaburro, Z.; Capasso, F. *Nano Lett.* **2012**, *12*, 6328−6333.
(24) Feng, L.; Liu, Z.; Lomakin, V.; Fainman, Y. *Appl. Phys. Lett.* **2010**, *96*, 041112.
(25) Zhao, Y.; Alù, A. *Phys. Rev. B* **2011**, *84*, 205428.
(26) Alù, A.; Engheta, N. *Structured Surfaces as Optical Metamaterials*; Cambridge University Press: New York, 2011.
(27) Auguie, B.; Barnes, W. L. *Phys. Rev. Lett.* **2008**, *101*, 143902.
(28) Silveirinha, M. G. *Phys. Rev. E* **2006**, *73*, 046612.
(29) Bohren, C. F.; Huffman, D. R. *Absorption and Scattering of Light by Small Particles*; John Wiley & Sons: New York, 1998.
(30) Zhao, Y.; Alù, A.; Engheta, N. *Metamaterials* **2011**, *5*, 90−96.
(31) Zhang, S.; Genov, D. A.; Wang, Y.; Liu, M.; Zhang, X. *Phys. Rev. Lett.* **2008**, *101*, 047401.
(32) Ekinci, Y.; Solak, H. H.; David, C.; Sigg, H. *Opt. Express* **2006**, *14*, 2323−2334.
(33) Alù, A.; Engheta, N. *Phys. Rev. Lett.* **2008**, *101*, 043901.
(34) Kobayashi, N. P.; Islam, M. S.; Wu, W.; Chaturvedi, P.; Fang, N. X.; Wang, S. Y.; Williams, R. S. *Nano Lett.* **2009**, *9*, 178−182.
(35) Ellenbogen, T.; Seo, K.; Crozier, K. B. *Nano Lett.* **2012**, *12*, 1026−1031.
(36) Johnson, P. B.; Christy, R. W. *Phys. Rev. B* **1972**, *6*, 4370−4379.